



LUND UNIVERSITY

A 10-mW mm-Wave Phase-Locked Loop With Improved Lock Time in 28-nm FD-SOI CMOS

Abdulaziz, Mohammed; Forsberg, Therese; Törmänen, Markus; Sjöland, Henrik.

Published in:

IEEE Transactions on Microwave Theory and Techniques

DOI:

[10.1109/TMTT.2019.2896566](https://doi.org/10.1109/TMTT.2019.2896566)

2019

Citation for published version:

Abdulaziz, T. Forsberg, M. Törmänen and H. Sjöland, "A 10-mW mm-Wave Phase-Locked Loop With Improved Lock Time in 28-nm FD-SOI CMOS," in *IEEE Transactions on Microwave Theory and Techniques*, vol. 67, no. 4, pp. 1588-1600, April 2019.

About this document

This is the version of this article that was accepted for publication, but not the final, published version.

General rights

Copyright and moral rights for the publications made accessible in the public portal are retained by the authors and/or other copyright owners and it is a condition of accessing publications that users recognise and abide by the legal requirements associated with these rights.

- Users may download and print one copy of any publication from the public portal for the purpose of private study or research.
- You may not further distribute the material or use it for any profit-making activity or commercial gain
- You may freely distribute the URL identifying the publication in the public portal

Take down policy

If you believe that this document breaches copyright please contact us providing details, and we will remove access to the work immediately and investigate your claim.

A 10 mW mm-Wave Phase-Locked Loop with Improved Lock Time in 28-nm FD-SOI CMOS

Mohammed Abdulaziz, *Member, IEEE*, Therese Forsberg, *Student Member, IEEE*, Markus Törmänen, *Senior Member, IEEE*, Henrik Sjöland, *Senior Member, IEEE*.

Abstract—This paper presents a millimeter-wave phase-locked loop (PLL), with an output frequency centered at 54.65 GHz. It demonstrates a mode-switching architecture that considerably improves the lock time, by seamlessly switching between a low-noise mode and a fast-locking mode that is only used during settling. The improvement is used to counteract the increased lock-time caused by cycle-slips that results from using a high reference frequency of 2280 MHz, which is several hundred times the loop bandwidth. Such a reference frequency alleviates the noise requirements on the PLL and is readily available in 5G systems, from the RF PLL. The millimeter-wave PLL is implemented in a low-power 28-nm FD-SOI CMOS process, and its active area is just 0.19 mm². The PLL also features a novel double injection-locked divide-by-3 circuit and a charge-pump mismatch compensation scheme, resulting in state-of-the-art power consumption and jitter performance in the low-noise mode. In this mode, the in-band phase noise is between -93 and -96 dBc/Hz across the tuning range, and the integrated jitter is between 176 and 212 fs. The total power consumption of the millimeter-wave PLL is only 10.1 mW, resulting in a best case PLL figure-of-merit (FOM) of -245 dB. The lock time in low-noise mode is up to 12 μ s, which is improved to 3 μ s by switching to the fast-locking mode, at the temporary expense of a power consumption increase to 15.1 mW, an integrated jitter increase to between 245 and 433 fs, and a FOM increase to between -235 and -240 dB.

Index Terms—60 GHz, 5G, charge pump, CMOS, divide-by-three, fast lock time, frequency synthesizer, ILFD, injection-locked divider, local oscillator, low phase noise, low-power, mm-wave, phase-locked loop, PLL.

I. INTRODUCTION

PHASE-LOCKED LOOP (PLL) frequency synthesizers are key parts of today's wireless transceivers, and designing PLLs for millimeter-wave (mm-wave) communication standards is challenging from many aspects. Their phase noise limits the highest achievable modulation order [1], and they also need to have fast settling and be able to operate at low power in battery operated devices [2]–[4]. In particular, fast

Manuscript received Month Date, 2018; revised Month Date, 2018; accepted Month Date, 2018. This paper was approved by Editor Name.

The first two authors contributed equally to this work.

This work was supported by the Swedish Research Council and the European Commission in the framework of the H2020-ICT-2014-2 project Flex5Gware (Grant agreement no. 671563).

M. Abdulaziz was with the Department of Electrical and Information Technology, Lund University, SE 221 00 Lund, Sweden and with the Department of Microtechnology and Nanoscience, Chalmers University of Technology, SE 412 96 Göteborg, Sweden. He is now with Ericsson Research, Ericsson AB, 223 62 Lund, Sweden (e-mail: mohammed.abdulaziz@ericsson.com).

T. Forsberg, M. Törmänen and H. Sjöland are with the Department of Electrical and Information Technology, Lund University, SE 221 00 Lund, Sweden. (e-mail: therese.forsberg@eit.lth.se, markus.tormanen@eit.lth.se, henrik.sjoland@eit.lth.se).

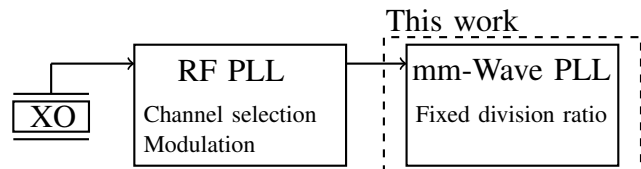


Fig. 1. Example of a mm-wave frequency generation architecture for 5G applications that utilizes the presence of an RF PLL.

settling time is required for communication standards that support very high data rates, to avoid losing large amounts of data during frequency locking. In frequency-modulated continuous-wave (FMCW) radar applications a fast settling PLL is required to be able to receive baseband signals at higher frequencies, and hence reduce the impact of the high flicker noise corner in short-channel technologies [3], [4].

A frequency synthesizer operating at about 60 GHz can be used for direct conversion transceivers in the unlicensed 60 GHz band, where for instance the WiGig/IEEE 802.11ad standard [2], future 5G standards [5], and high precision radars [3] will reside. Such a frequency synthesizer, followed by a divide-by-2 circuit, can also be used to generate quadrature signals for 28 GHz front-ends intended for emerging 5G applications. It can also be used as the local oscillator (LO) in dual-frequency conversion transceivers, by using the 60 GHz PLL output signal together with the divided 30 GHz or 20 GHz signals present in the PLL, depending on whether the first division step after the voltage controlled oscillator (VCO) divides by 2 or 3. Higher frequencies in the E-band can then be targeted. Clearly, high performance and low cost 60 GHz PLLs have many potential applications.

The anticipated 5G wireless communication systems will support mm-wave links together with lower frequency cellular ones. This means that a mm-wave PLL operating with a high reference frequency (f_{REF}) may have another PLL as its input, instead of a crystal oscillator (XO). This has been the case in recent works and prior art, such as [6]–[8]. Similarly, a radio frequency (RF) f_{REF} can be provided by direct digital synthesis, which has been demonstrated in several state-of-the-art sub-millimeter frequency imaging radar systems [9]–[11]. Increasing f_{REF} is beneficial for the PLL noise performance, because when the f_{REF} noise is added to the PLL in-band noise it is first multiplied by the PLL division ratio squared. If the loop bandwidth is kept low, a PLL with high f_{REF} may also decrease the current consumption in the charge pump (CP). However, if not addressed properly, this approach will inevitably lead to problems with prolonged settling time. An additional advantage of using the PLL for cellular bands as

an input to the mm-wave PLL in 5G systems, is that the RF PLL can provide the fine-grain resolution required for channel selection and/or modulation and thus simplify the design of the mm-wave PLL. The architecture of such a system is shown in Fig. 1.

In this paper a new PLL architecture is presented. Tuned to 55 GHz, the PLL is aimed at 5G applications, but it also has the more general goal of demonstrating an architecture that balances low noise, low power consumption and fast settling time, when a restriction is that the f_{REF} is several hundreds times the PLL loop bandwidth. The demonstrated PLL also features a novel double injection-locked divide-by-3 circuit, that achieves a wide lock range at low current consumption. Furthermore, the CP includes a novel current mismatch mitigation technique based on negative feedback. To support rail-to-rail output signals and hence wider VCO frequency range, the CP also features an improved operational amplifier that allows operation over a large common-mode range. The presented PLL shows competitive performance at a power consumption of just 10.1 mW, a value which to our knowledge is the lowest presented at such high output frequency. The PLL architecture is first introduced in Section II. Detailed description of circuit design is then presented in Section III. The measurement results together with a comparison to the state-of-the-art are then presented in Section IV. Finally, the paper is concluded in Section V.

II. PLL ARCHITECTURE

A conventional type-II PLL is shown in Fig. 3(a). Increasing f_{REF} is an effective technique to achieve lower phase noise [6]–[8]. Traditionally, using a higher f_{REF} means that the loop bandwidth can be higher, which in turn leads to an improved lock time. However, when the reference frequency becomes very high, the loop bandwidth is no longer limited by the reference frequency. Instead, if minimum jitter is targeted, the loop bandwidth should be chosen as the frequency where the VCO phase noise and extrapolated in-band phase noise at the PLL output intersect. Generally, for state-of-the-art mm-wave PLLs a typical bandwidth for optimum noise performance is in the order of a few MHz. If f_{REF} is then chosen to be about 2 GHz, the ratio of f_{REF} to loop bandwidth becomes very high. To still get the desired bandwidth when using such a high f_{REF} , either the loop filter (LF) capacitances must be increased, or the charge pump current (I_{CP}) must be reduced. Increasing the size of the LF leads to a large area for the capacitors, while reducing I_{CP} is an attractive way of reducing the overall power consumption. However, this will also limit the available output current from the CP that charges the filter capacitances, and the PLL lock time will be severely degraded due to so-called cycle slips, originating from nonlinear effects in the transient when the PLL is out of lock-in range [12]. An example of this is shown in Fig. 2, where the simulated VCO control voltage settling behavior for two PLLs with the same bandwidth is presented. One uses an f_{REF} that is 8 times higher, and to keep the loop bandwidth unchanged the I_{CP} is then also reduced 8 times. In the case of a high f_{REF} -to-bandwidth ratio, it can be seen that the cycle-slips prevents

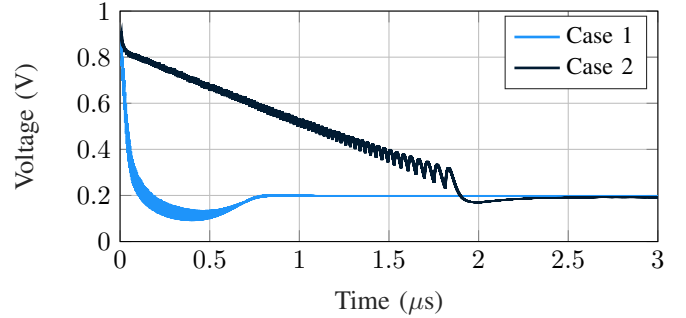


Fig. 2. Example of the impact of cycle-slips. Both cases have the same loop bandwidth, but f_{REF} is 8 times larger and I_{CP} is 8 times smaller in case 2.

the PLL from approaching the correct frequency exponentially, and that the settling time is significantly prolonged.

It is thus clear that aggressively increasing the f_{REF} to obtain better noise performance affects the settling time, and that low phase noise and fast settling time are contradictory in this case. To solve this conflict of requirements we propose a PLL architecture that can achieve fast settling by disregarding the noise performance during PLL settling, and then seamlessly shift to a low noise mode at steady state, thereby achieving both fast settling and low noise. The proposed PLL architecture, that features two such optimized modes of operation, is shown in Fig.3(b). Fast settling mode is enabled when SW_{fast} is set to logic 1. Both multiplexers then forward the signal divided by an extra factor N_2 . The effective reference frequency becomes f_{REF}/N_2 , and the divided VCO frequency to be compared to it by the phase frequency detector (PFD) becomes $\frac{f_{VCO}}{N_1 N_2}$. At the same time, the amplitude of the current pulses fed to the loop filter from the CP become $N_2 I_{CP}$. This mode has an increased maximum current that can charge the capacitors in the loop filter, which yields a faster settling. Low noise mode is enabled when setting SW_{fast} to logic 0. Both multiplexers then forward f_{REF} and f_{VCO}/N_1 without the extra division. The amplitude of the CP current pulses is at the same time reduced to I_{CP} . The reduced CP current increases the settling time, but the total power consumption is reduced and the decrease in total division ratio improves the in-band phase noise of the PLL. In this work, f_{REF}/N_2 is chosen to be 8, large enough to demonstrate the efficiency of the mode-switching architecture.

It is important to note that for either mode setting, the small signal PLL characteristics remain the same. One CP is switched on or off, but a seamless transition between modes is possible because the steady state value of V_{ctrl} is the same in both modes and no loop filter reconfiguration is needed. The signal SW_{fast} can be easily generated when the current operating frequency is to be changed. As will be demonstrated by measurements in Section IV, the mode transition will indeed be seamless and not generate any sudden transients. Therefore, the mode change back to low-noise mode can be performed simply after a predefined delay, without any need of calibration. As the measurements in Section IV suggest, a safe choice for the delay is around 2.5 μ s.

An alternative to the fast-settling PLL mode would be to use a fast digital oscillator calibration, in both cases followed

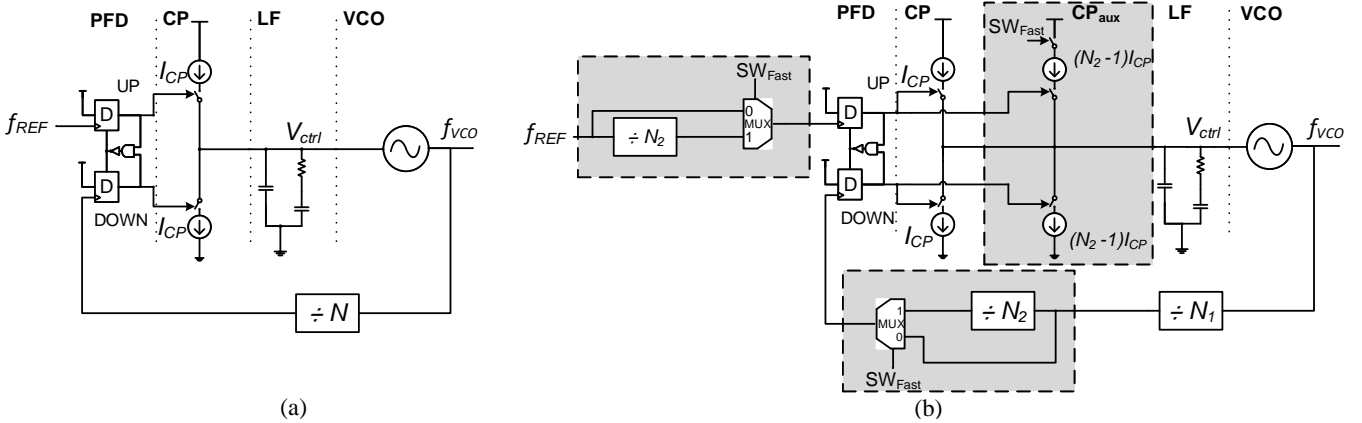


Fig. 3. Schematics of (a) a type II PLL and (b) the proposed PLL architecture, where $SW_{fast} = 1$ activates fast-locking mode, and $SW_{fast} = 0$ activates the low-noise mode.

by linear settling. In [13] such a technique is used, with a successive approximation register. The frequency divider of the PLL is then set to the target value, and the divided frequency with different digital oscillator control words is measured using a counter. The time of the counting is proportional to the required precision. For instance, using 7-bit precision to provide margin against cycle slips in the low-noise mode requires counting about $2^7 = 128$ cycles. Since the clocks are not synchronized, an error of up to one cycle can occur [13]. This means that the measurement interval must be doubled. With a 2-GHz clock, each measurement will then require 128 ns. With a 7-bit control word, 7 such measurements are needed, i.e. one per bit. The total calibration time will then be about $0.9 \mu\text{s}$. As can be seen in [13], the linear settling following the calibration will then have a significant transient and require additional time, compared to the proposed technique that is close to transient-free. All in all, it seems the two techniques can provide similar settling times. However, implementing the digital frequency tuning in the oscillator to support the calibration would result in increased complexity and parasitics in the sensitive mm-wave oscillator. The overall circuit simplicity and robustness of operation is a key advantage of the proposed technique.

III. PLL IMPLEMENTATION AND CIRCUIT DETAILS

A. The VCO and divider chain

The PLL was implemented in a low power 28-nm CMOS SOI process. The VCO and divider chain is shown in Fig. 4. The phase noise performance of the cross-coupled pair VCO is improved by using the tail current filtering technique [14], which is effective also at 60 GHz [15]. The VCO output is fed differentially to an injection-locked frequency divide-by-3 circuit (ILFD), as well as to two single-ended buffers, for measurement purposes. Simulations show that the full differential VCO voltage swing of 2.7 V peak-to-peak can be preserved, even if the VCO output signal is also required to drive additional, mainly capacitive loads, such as divide-by-two ILFD circuits or a mixer. The differential output of the ILFD is fed directly to a differential latch-based divide-by-2 circuit, followed by true single phase clock (TSPC) dividers

and a multiplexer [16]. The first stage of the TSPC divider divides the frequency of the input by 4 or 6, depending on if the Sel control signal is set to logic 0 or 1, respectively. This signal is used to perform step response measurements. Based on whether the PLL is to operate in low-noise mode or fast-settling mode, the control signal SW_{fast} is set to either logic 1 or 0. The sinusoidal reference signal is buffered and converted to a square wave on chip, and fed to the PFD through a multiplexer in a similar configuration as in the divider chain path.

For mm-wave PLLs it is preferable to use a division ratio higher than two in the first feedback divider stage after the VCO, if it can be achieved without increasing the power budget. At such frequencies, however, as explored in [17], [18], special architectures suited for mm-wave operation have to be employed. One such architecture that has lately gained increased attention due to its attractive properties, such as low power consumption and small area, is the mm-wave dynamic current mode logic (DCML) divider. The operation at mm-wave frequencies is attributed to that the memory elements in the latches are the parasitic capacitances of the active devices. Unfortunately, this kind of divider is sensitive to process, voltage and temperature (PVT) variations. Injection locking is a more attractive technique in terms of robustness, since LC tanks are then used to tune the divided frequency output, and ILFDs with higher division ratios such as 3 have been demonstrated [19]–[21]. However, current consumption and locking range remain major concerns when increasing the division ratio, due to less effective current injection. The ILFD presented in this work addresses these issues.

Differential ILFD divide-by-two operation is typically based on injecting a current signal at a frequency close to the second harmonic of the ILFD LC resonance (f_0), at the source of the current commutation MOS pair, as shown in Fig. 5(a) [22]. The current signal is then injected by the tail transistor M_1 which acts as a transconductance. Note that M_2 and M_3 act as a single balanced mixer with a maximum conversion gain of $G = \frac{2}{\pi}$, down-converting the injected signal to a frequency close to f_0 at the LC tank. A more general observation is that injection locking division is achieved by injecting a harmonic signal to the circuit that by some mechanism results in a

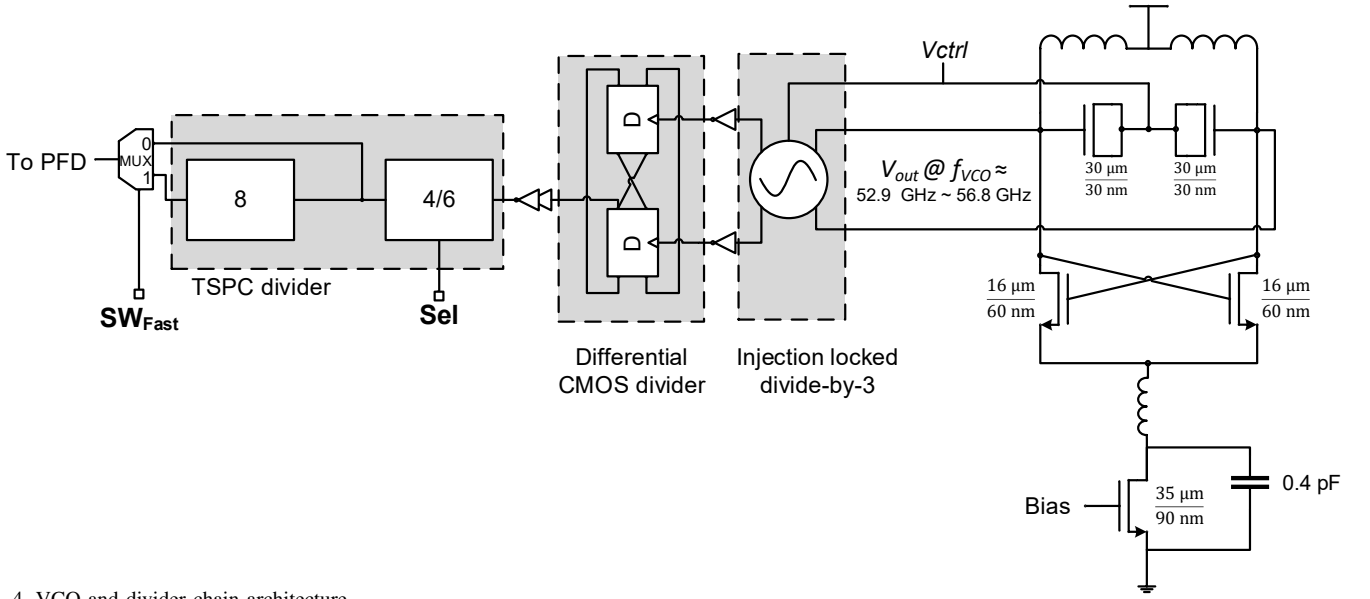


Fig. 4. VCO and divider chain architecture.

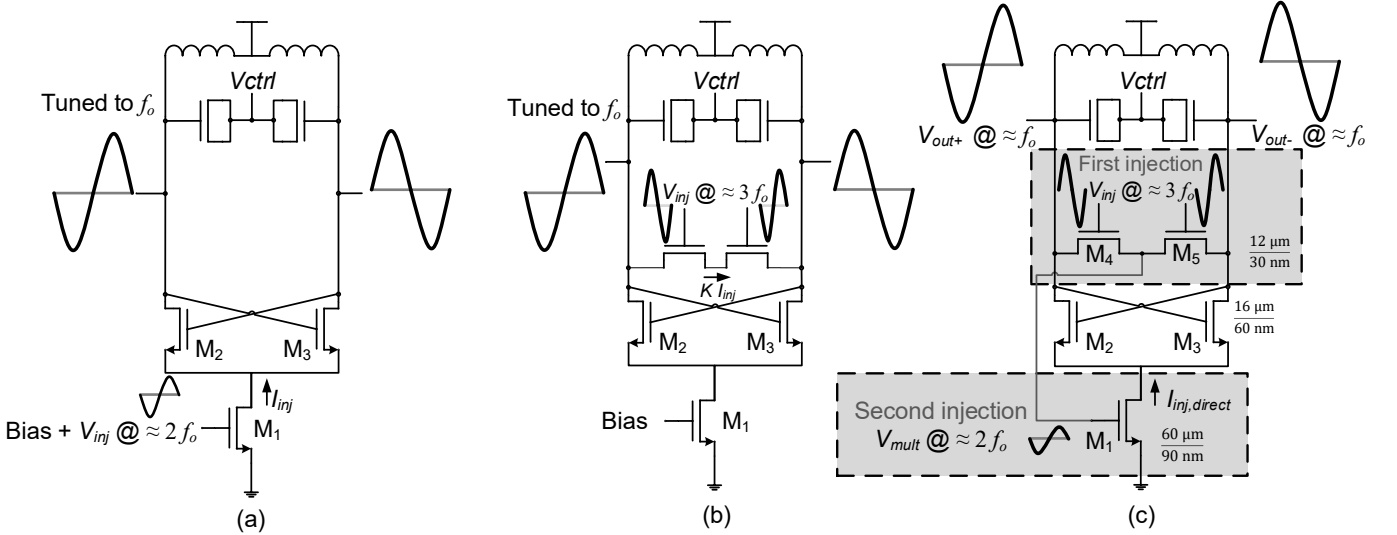


Fig. 5. Injection-locked frequency dividers. (a) Divide-by-2. (b) Divide-by-3. (c) Proposed novel double injection divide-by-3.

current signal at the drains of M_2 and M_3 , with a frequency close to f_0 and a magnitude sufficiently large to pull the oscillator to that frequency. An upper bound of the frequency locking range for the ILFD shown in Fig. 5(a) is expressed by [22], [23]

$$\omega_{range} \leq \frac{\omega_0}{2Q} \cdot \frac{2}{\pi} \cdot \frac{I_{inj}}{I_{osc}} \quad (1)$$

where Q is the quality factor of the divider's LC tank, I_{inj} the magnitude of the injected current, and I_{osc} the magnitude of the free running oscillator current at f_0 . In (1) $G = \frac{2}{\pi}$ is used assuming M_2 and M_3 switch on/off abruptly [23]. Injecting a voltage V_{inj} at the gate of M_1 makes the frequency locking range ω_{range} become

$$\omega_{range} \leq \frac{\omega_0}{2Q} \cdot \frac{2}{\pi} \cdot \frac{G_m \cdot V_{inj}}{I_{osc}} \quad (2)$$

It is important to note that ω_{range} is referred to the output frequency of the divider. Clearly, a way to improve the lock range

without compromising performance, such as reducing Q , is by maximizing I_{inj} (i.e. increasing the injection efficiency).

To make the ILFD to divide by 3, the current can be injected directly to the output using differential back-to-back MOS devices, as shown in Fig. 5(b) [21], [24]. In this work a novel double injection-locked divide-by-3 circuit is proposed, see Fig. 5(c). The proposed divider uses double injection to achieve increased injection efficiency, enabling a wide tuning range at a reduced current consumption. The triode-multiplier constituted by devices M_4 and M_5 multiplies the injected voltage (V_{inj}) at frequency $f \approx 3f_0$ with that of the divider output, tuned to f_0 . It was shown in [25] that the output voltage of the triode-multiplier is comprised of even order harmonics. In this case, the multiplier is excited with rail-to-rail signals from the VCO and therefore it acts as an efficient voltage-mode single-balanced mixer with a differential input and a single-ended output. The output of the multiplier is simply the even order inter-modulation terms, which in locked state are at

frequencies close to $2f_o$, $4f_o$ and higher even order harmonics. These tones are in turn fed to the tail current device, which acts as a transconductance that injects current mainly at $\approx 2f_o$ to the source of the active pair (M_2 and M_3). This results in an additional injection mechanism similar to that of the divide-by-2 ILFD shown in Fig. 5(a). Higher order harmonics are not significant, as they are suppressed by the circuit. The triode-multiplier also injects a current signal at the first harmonic, $I_{inj,direct}$ directly to the output. Hence, the lock range of the divider is proportional to the sum of lock ranges of the two dividers in Fig. 5(a) and 5(b). Including the transfer of the passive mixer $V_{inj} = \frac{2}{\pi}V_{out}$ in (2) and adding the direct injection gives

$$\omega_{range} \leq \frac{\omega_0}{2Q} \cdot \left(\frac{2}{\pi^2} \cdot \frac{g_m V_{out}}{I_{osc}} + \frac{I_{inj,direct}}{I_{osc}} \right) \quad (3)$$

Equation (3) presents an upper bound to the lock range of the double injection-locked divider, indicating that the lock range can be increased considerably compared to the direct-injection-only circuit, without any current penalty. The current budget can also be reduced significantly, since with the second injection path established, the first injection devices (M_4 and M_5 in Fig. 5(c)) can be small, increasing the LC resonator impedance. Further efficiency enhancement is also achieved due to the push-push regime that the tail current source M_1 is operated in.

The designed divider covers the frequency range of the VCO with a margin, to account for PVT variations. Simulations of the divider sensitivity with single injection and with the proposed double injection are shown in Fig. 6. At the same power consumption, with an input power of 5 dBm and at a fixed varactor voltage of $V_{DD}/2$, the double injection increases the locking range from 2.5% to 8.5%, i.e. by a factor of 3.4. All possible spurs created by the ILFD are harmonics of the divided signal and, since the output is differential, the odd order harmonics dominate. Directly after the ILFD are inverting buffers that aim to make the signal even more square-wave shaped and thus increase the odd harmonics even further. The spurs of the ILFD are thus of little concern in this case. The simulated phase noise of the ILFD at 10 MHz offset from the carrier is below -141 dBc/Hz, with a noise of -146 dBc/Hz close to its self-resonance frequency.

The ILFD is followed by a divide-by-2 circuit as shown in Fig. 5 (a). The latch proposed in [26], shown in Fig. 7, can be used directly after the ILFD thanks to the high speed 28-nm technology, while the last divider stages are implemented in TSPC logic.

B. The PFD-CP

The three-state PFD used in this work is TSPC-based and produces UP/DOWN pulses, which are converted to differential signals by inverters. Transmission gates are used to match the inverter delay, thereby mitigating imbalance between the differential signals.

The CP schematic is shown in Fig. 8, using a differential architecture ($M_1 - M_6$) for high speed and reduced charge sharing. The UP/DOWN currents are matched to a first order through a 1:1 current mirror ($M_1, M_6, M_{11} - M_{13}$). Due to the

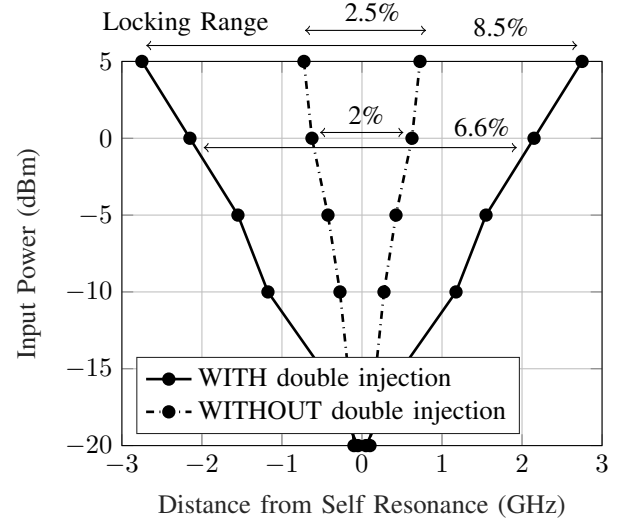


Fig. 6. The simulated sensitivity of the ILFD at a fixed varactor voltage of $V_{DD}/2$, with and without the double injection, at the same power consumption.

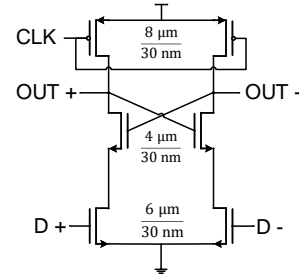


Fig. 7. Differential high speed CMOS latch.

reduced feature size, however, the channel length modulation causes mismatch between the UP and DOWN currents at high and low values of the output voltage V_{ctrl} . This results in different UP and DOWN pulse widths at steady state, where the pulse with less current must become wider to compensate for the current difference and produce zero net charge to the LF. This issue results in increased spur levels and noise contribution from the CP, as described below.

In [28], [29] it was shown that high frequency noise folding due to CP gain mismatch can result in large PLL in-band phase noise increase, especially in fractional-N PLLs with strong $\Sigma\Delta$ -modulation noise. This effect is even more pronounced by charge injection, further increasing gain mismatch in the cross-over region, resulting in more noise folding. To reduce charge injection, an operational amplifier OPI is therefore used to make the voltage of the dummy node in the differential CP track V_{ctrl} [30]. Furthermore, with increased f_{REF} , the contribution of the CP to the PLL phase noise becomes more significant. This in-band contribution is [31], [32]:

$$\mathcal{L}_{CP} = \frac{2k_B T \gamma g_m n_T}{(I_{CP}/2\pi)^2} \cdot (T_p/T_{REF}) \cdot \left(1 + \frac{(T_p/T_{REF})f_c}{f_{offset}}\right) \cdot N^2 \quad (4)$$

where $T_{REF} = 1/f_{REF}$, k_B is the Boltzmann constant, T the absolute temperature, γ the MOS gamma factor, g_m the transconductance of the devices in the 1:1 current mirror, n_T the number of MOS devices used to copy current to the CP, f_c

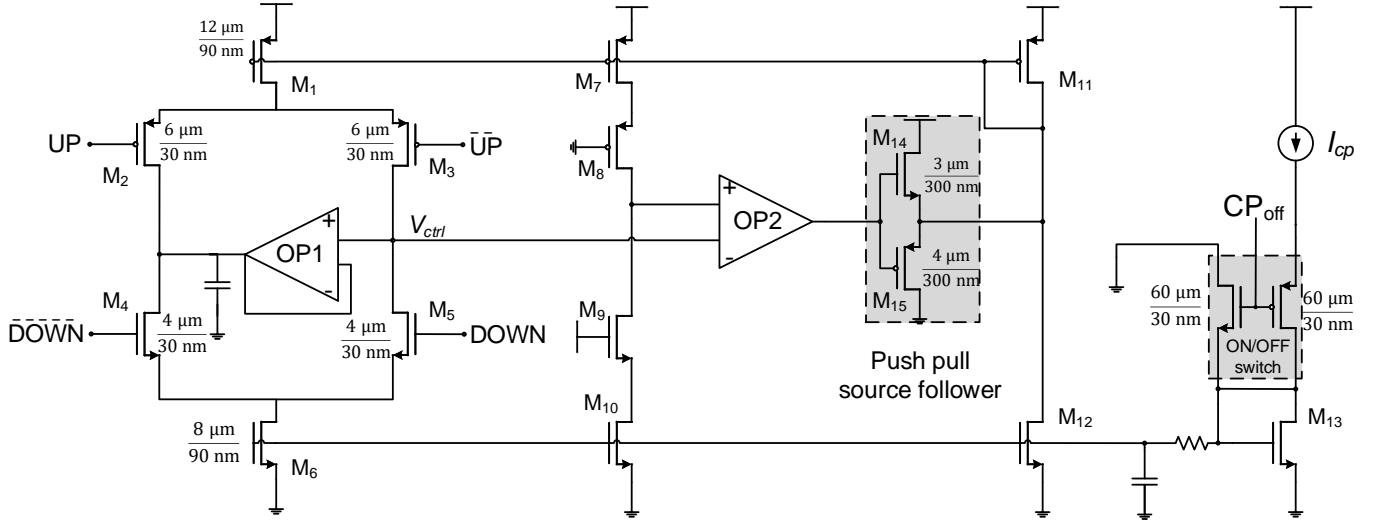


Fig. 8. Schematic of the charge pump with replica-based feedback loop to correct for UP/DOWN current mismatch.

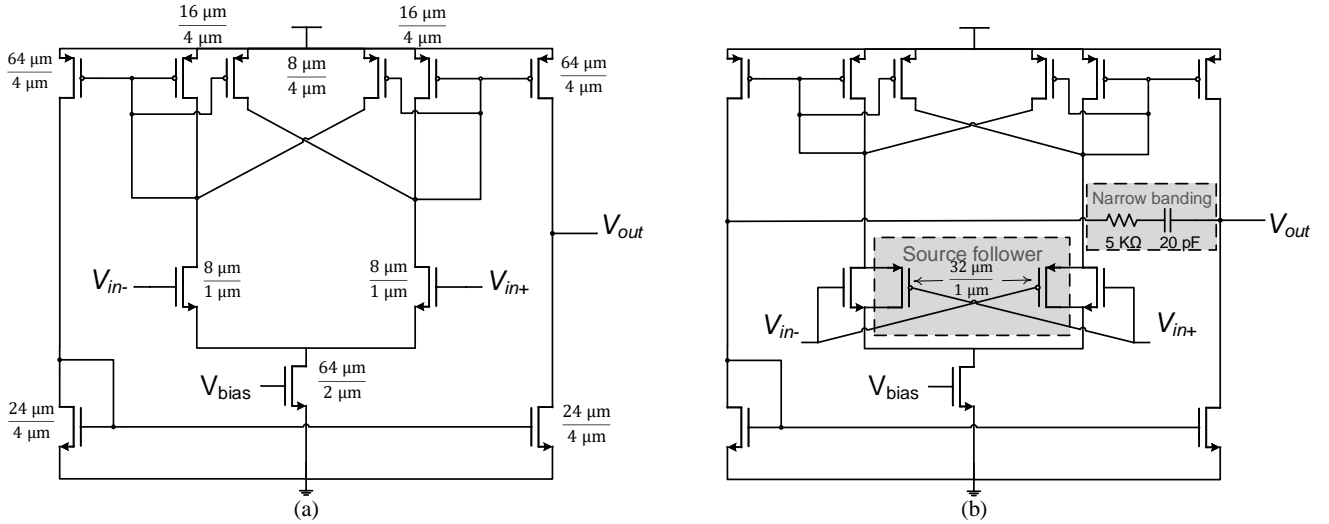


Fig. 9. (a) The amplifier proposed in [27] and (b) improved amplifier with parallel source follower stage for rail-to-rail common-mode operation and RC narrow-banding for loop stability.

the $1/f$ noise corner of the MOS devices, and T_p the current pulse width in steady state (in this work $T_p \approx 20$ ps). This relation indicates that the noise contribution of the CP remains constant if I_{CP} is scaled down by the same factor as the PLL division ratio N . However, T_p is dependent on the speed of the latches in the PFD and hence do not scale with f_{REF} . As T_{REF} is reduced the CP phase noise contribution will therefore increase, both thermal noise and even more so $1/f$ noise. A mismatch in UP/DOWN currents will result in wider pulses, as the minimum pulse width is set by the PFD reset delay. The pulses will then contain more charge and contribute more phase noise. There are thus two mechanisms that cause increased phase noise due to CP mismatch, high frequency noise folding and loop filter noise injection, motivating a technique to counteract mismatch.

To reduce the mismatch between UP and DOWN currents, compensation of the channel length modulation effect is required [33]. The schematic of the CP is shown in Fig. 8, where an additional dc current branch ($M_7 - M_{10}$) has been

introduced, with 1:1 replicas of (M_1, M_3, M_5, M_6). A negative feedback loop, using amplifier OP2 with a push-pull output stage (M_{14}, M_{15}), controls the UP current so that the dc current branch outputs V_{ctrl} . Since the NMOS and PMOS currents are equal in the dc branch, and it has the same output voltage as the CP, and replicated devices, the UP and DOWN currents must also be equal.

The operational amplifiers used in the CP needs to have high gain as well as capability to handle rail-to-rail common-mode signal levels. This is crucial as the CP output voltage range limits the PLL frequency range. The schematic of a conventional amplifier proposed in [27] is shown in Fig. 9(a). All the devices are biased in weak inversion for low current consumption, keeping in mind that only low frequency signals are processed. The input differential pair limits the minimum common-mode input voltage, and an improved version is shown in Fig. 9(b), where the input stage is a differential pair in parallel with a differential cross-coupled PMOS source follower. As the common mode input voltage drops below a threshold voltage, the common source gain is drastically

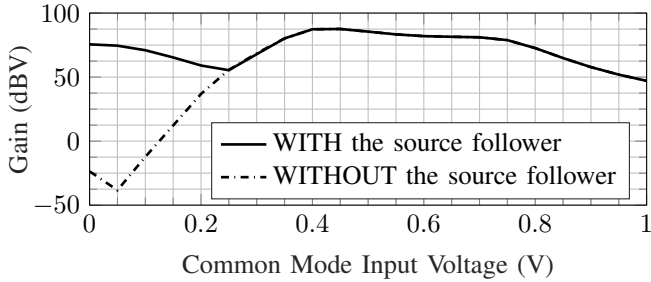


Fig. 10. Simulated low-frequency gain of the amplifier in Fig. 9, with and without the parallel source follower.

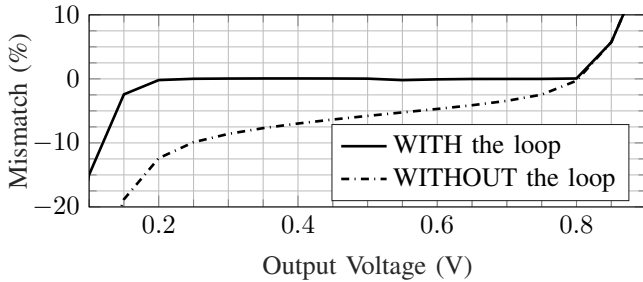


Fig. 11. Simulated CP current mismatch, with and without feedback loop, at 1 V supply.

reduced. However, inserting the PMOS source follower in parallel, which turns on under these conditions, preserves some of the gain. Since the differential pair common source amplifiers are loaded with diode connected devices, the voltage gain from the gate to drain is not high, making the gain of the common source and the source follower more similar. This technique has also been used in [25] to improve the linearity of operational transconductance amplifiers. Simulation of the voltage gain with and without the proposed technique is shown in Fig. 10. As can be seen in the figure, using a PMOS source follower helps providing gain even at 0 V common-mode input. Traditionally the amplifier shown in Fig. 9(a) has been used without phase compensation, however, in this case the high gain of the dc loop required compensation, realized by the resistor-capacitor link at the output. The 20 pF capacitor creates a dominant pole, and the resistor a high frequency zero, advancing the phase.

The CP was simulated when driven by two in-phase signals with a frequency of 2 GHz, to resemble the PLL locked state with *DIV* and *REF* matched in phase and frequency. The CP output was forced to a fixed voltage and the output current was observed. The net output current then represents the mismatch between UP and DOWN currents. The simulated mismatch versus CP output voltage with/without the proposed CP mismatch correction loop is shown in Fig. 11. As can be seen, the current mismatch is reduced to less than 0.1% in the range from 0.2 V to 0.8 V. The excessive mismatch near supply (1 V) and ground voltage proximity is due to the V_{dsat} drop required over the tail current devices M_1 and M_6 shown in Fig. 8.

IV. MEASUREMENT RESULTS

Before designing the complete PLL, a stand-alone ILFD was designed and fabricated. For comparison it shares a chip with an identical ILFD - but without the double injection path.

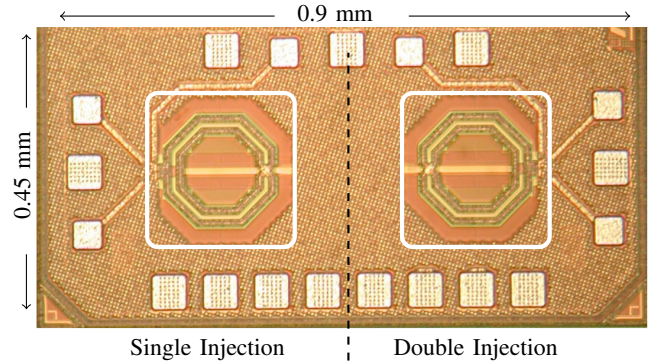


Fig. 12. ILFD chip photo. The active area is inside the white rectangles.

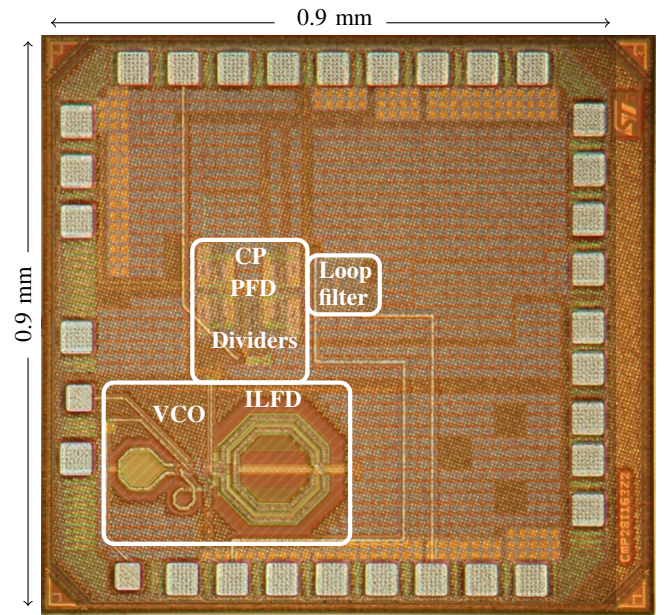


Fig. 13. The chip micrograph with the layout overlaid. The active area of 0.17 mm² is inside the white rectangles.

Both the ILFDs and the subsequent PLL were fabricated in the STMicroelectronics 28-nm ultra-thin body and buried oxide (UTBB) fully-depleted (FD) silicon on insulator (SOI) CMOS process with 10 metal layers for interconnect, and with the metal-insulator-metal (MIM) capacitance option. The active area of each divider is 0.05 mm² and the total area of the PLL chip is 0.9 x 0.9 mm², of which the active area is just 0.17 mm². The ILFD die microphotograph is shown in Fig. 12, and that of the PLL chip overlaid with a layout image in Fig. 13. Both chips were mounted on FR-4 printed circuit boards, to which all needed supply, bias and signal pads were wire-bonded. Only the mm-wave signals were probed, using Infinity microprobes from Cascade Microtech. The PLL measurement setup is depicted in Fig. 14. The input reference frequency was generated by an Agilent E4438C signal generator with low-noise option UNJ. For the phase noise measurements, an FSWP phase noise from Rohde & Schwarz with harmonic mixers for the 50 to 75 GHz band was used. The FSWP also provided the setup with low-noise supply voltages. An FSU50 spectrum analyzer with a harmonic mixer, also from Rohde & Schwarz, was used for the output spectrum measurements. The loop control voltage measurements used a 4 GHz 20 GS/s Rohde & Schwarz RTO 1044 digital oscilloscope. Pulses

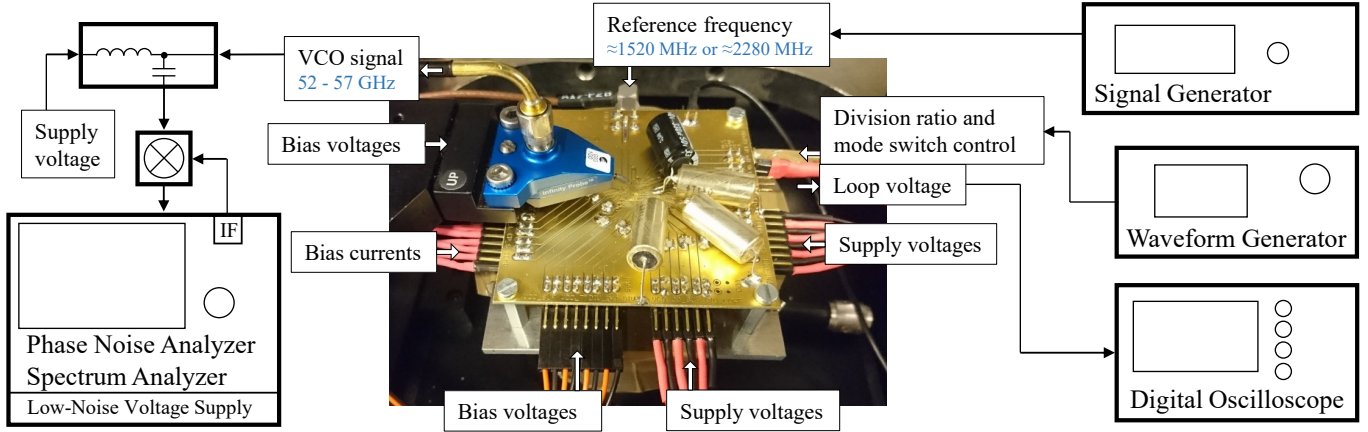


Fig. 14. The PLL measurement setup.

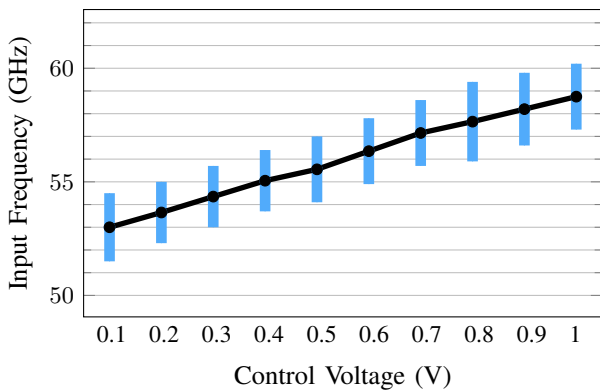


Fig. 15. Measured locking range at a power consumption of 2.5 mW for the double injection version of the ILFD.

for the mode switch control were generated by a WW2572A 250 MS/s waveform generator from Tabor Electronics. To not introduce noise on the sensitive loop control voltage node, the oscilloscope was disconnected during phase noise measurements.

Measurement results from the the ILFD are shown in Fig. 15, and the two versions are compared in Table I. When utilizing the full range of the varactor, the measured locking range is increased from 13% for the single injection circuit, to 17.5% for the double injection circuit. Even if these ILFD measurements use less than 0 dBm input signal due to measurement setup limitations, which is less than the expected VCO output voltage in the PLL, also the single-injection ILFD demonstrates a wide locking range covering the VCO frequencies. However, using the single injection ILFD in the PLL would allow for almost no drift in tuning due to process and temperature variations between the VCO and the ILFD. Since they will be tuned together by the same control voltage, the key concern is how sensitive the mm-wave parts of the PLL are to unforeseen tuning mismatch, and the robustness is dependent on the locking range of the ILFD for a fixed varactor control voltage. At a fixed varactor voltage of $V_{DD}/2$, measurements show that the double injection technique increases the lock range by more than a factor of two, from 2.4% to 5.2%.

When measuring the PLL, deviations from simulated performance were found. One such difference was that the out-

TABLE I
COMPARISON BETWEEN MEASURED RESULTS FOR THE SINGLE AND DOUBLE INJECTION CIRCUITS

At approximately 0 dBm input power	Single injection	Double injection
Locking range at 2.5 mW	53 - 60.5 GHz (13%)	52.8 - 62.9 GHz (17.5%)
Locking range at 1.5 mW	54 - 60.9 GHz (12%)	53.5 - 62 GHz (15%)
Locking range at 2.5 mW when $V_{varactor} = V_{DD}/2$	54.1 - 55.4 GHz (2.4%)	54.1 - 57 GHz (5.2%)

of-band noise was worse than anticipated from measurements of earlier stand-alone VCOs in the same CMOS process [15], possibly due to the decision to use a single ended output buffer for the VCO signal, or due to noise coupling to the loop control voltage node. This was addressed by increasing the PLL bandwidth. The in-band noise was also higher than expected from simulations, which was alleviated by the decision to increase the CP current, and to complement the internal loop filter with additional capacitance, connected externally. The choice of external components was a capacitor twice the size of the internal one, in series to ground with a resistor half the size of the internal one. If implemented on chip, the extra loop filter would add approximately 0.02 mm² of active area, making the new total active area 0.19 mm².

All PLL performance measurements were taken using the same settings applied to a single chip in room temperature. Subsets of the full measurement set were also taken on three additional chips, to investigate variations between samples. The supply voltages for the VCO, ILFD, 20 GHz latch, and the output buffer were set to 0.8 V, and the supply voltages for the low frequency dividers, PFD, CP and CP amplifiers were set to 1.06 V. The regular and large CP currents were set to 300 μ A and $7 \times 300 = 2400 \mu$ A, respectively. The total power consumption of the PLL was then measured to 15.2 mW in fast-locking mode, and 10.1 mW in low-noise mode. The measured power consumption of each contributor is visualized in Fig. 16. It is apparent that the CP current results in a significant power consumption reduction when the PLL operates in low-noise mode. However, the full effect cannot be clearly seen in the figure since the CP shares supply with the PFD, which in low-noise mode will operate at a

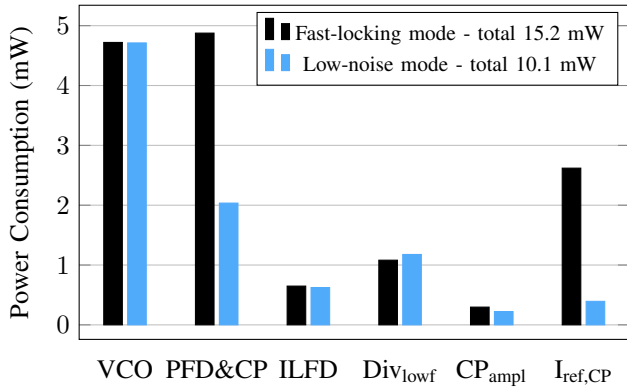
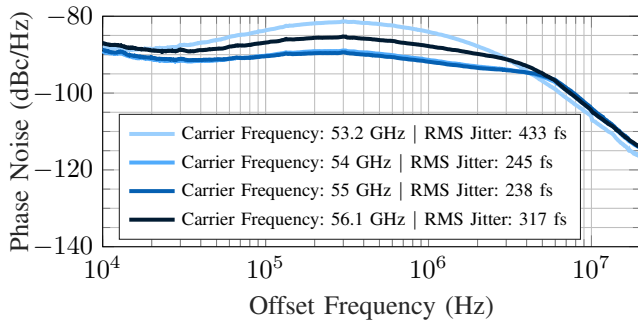
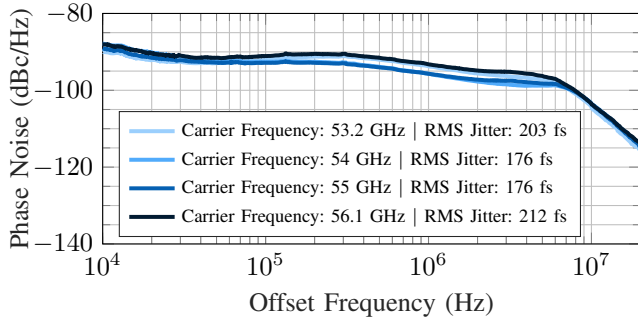


Fig. 16. Measured power consumption of each contributor in low-noise and fast-locking mode.



(a)



(b)

Fig. 17. Measured phase noise of the PLL in (a) fast-locking mode and (b) low-noise mode.

frequency 8 times higher, hence consuming more power. Since the PLL will be in low-noise mode nearly all the time, the power in low-noise mode will be presented as the PLL power consumption.

The PLL frequency range, i.e. the range where the PLL is able to acquire lock, was measured to 52.87 to 56.81 GHz. At the edges of this range, however, the reduced CP and VCO gain reduce the PLL bandwidth, which along with increased CP current mismatch result in degraded phase noise performance. Hence, the useful frequency range of the PLL is therefore where the phase noise performance is relatively uniform. This was measured to be between 53.2 and 56.1 GHz, a 5.3% range, in which the jitter deviated by less than 1.6 dB from the minimum value of 176 fs, see Fig. 17. While the measured tuning range, which is 1.45 GHz when divided by two, is wide enough to cover the upcoming 5G band in the USA, that is 0.85 GHz located between 27.5 and 28.35 GHz

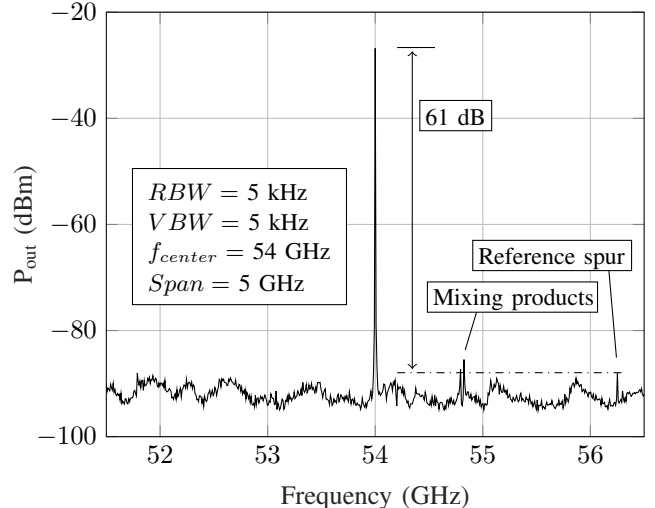


Fig. 18. Measured PLL output spectrum in low-noise mode, with a division ratio of 24. The mixing products and undulating noise floor are due to the harmonic mixer of the spectrum analyzer.

[5], it still requires some slight tuning. To ensure that the intended bands are covered even in the presence of process variations, the PLL frequency range could be increased. An increased PLL output frequency range will also have the added benefit of making the PLL useful in more applications. The output frequency range of the presented PLL is mainly defined by VCO tuning range. The most straight-forward way to increase this is to increase the VCO varactor size or to include switched capacitor arrays in the VCO tank, resulting in a trade-off between phase-noise and tuning range.

The output spectrum at a PLL output frequency of 54 GHz was measured, see Fig. 18. The PLL was in low-noise mode and the total division ratio of the PLL was set to 24. To access the differential VCO signal outside the chip it was fed to two single-ended on-chip buffers, one of which was accessible by on-chip probing. The buffers were sized down to produce a signal of lower power, to reduce coupling to sensitive parts of the circuit, as well as supply ripple due to high frequency current through bond wires. Because of this, the measured off-chip output signal power was about -27 dBm. Note that this is just for measurement purposes, and that the PLL is intended to deliver its output signal to a transceiver on the same chip. Since the measurement setup lacked external amplifiers and the used external mixer has high signal loss, the measured spectrum has a high noise floor. As can be seen in the PLL output spectrum in Fig. 18, the external harmonic mixer also makes the noise floor itself undulate, and creates spurs. The reference spurs, at a distance of 2.25 GHz from the carrier, are measured to be below -61 dBc.

The PLL phase noise measurements in Fig. 17 show the phase noise and RMS jitter across the PLL frequency range, in low-noise and fast-locking mode. The total division ratio was set to 24, by setting the *Sel* signal in Fig. 4 to a logic 0. The RMS jitter was calculated from the measurements by integrating phase noise from 1 kHz to 30 MHz offset frequency. The best measured phase noise performance was at an output frequency of 54 GHz, where the RMS jitter was 176 fs and the phase noise at 1 MHz and 10 MHz offset

TABLE II
PLL PERFORMANCE SUMMARY AND COMPARISON TO STATE-OF-THE-ART MM-WAVE CMOS PLLS

Ref.	CMOS Tech. (nm)	Type	Ref. Freq. (MHz)	Power (mW)	Phase Noise @1MHz (dBc/Hz)	RMS Jitter (fs)	Lock Time (μ s)	Center Freq. (GHz)	Freq. Range (%)	Core Area (mm ²)	Ref. Spur (dBc)	FOM _{PLL} ¹ (dB)
[34]	65	Fund. LO	135	24.6	-89.9 to -91.5	-	$> 5^2$	63.1	16.5	0.192	-54.5	-
[35]	40	Subsampling PLL	40	42	-88 to -92	200 to 350	-	58.5	16.2	0.16	-40	-207.7 to -202.9
[36] ³	65	Time-to-digital converter all digital PLL	100	48	-90	590.2	3	60	11.7	0.48	-74	-228
[37]	28	Fund. LO, frac. N 24 GHz PLL + 60 GHz QILO	27	107	-93.8 to -96.5	900 ²	-	59.4	18.2	0.294	-	-221
[38]	65	All digital PLL	100	46	-88 to -94.5	223 to 302.5	$< 1^4$	58	27	0.45	-48.3 / -52.2 ⁵	-236 to -233
[39]	65	Subsampling 20 GHz PLL + 60 GHz QILO	36 or 40	32	-92 ²	290	-	60.4	16	1.08 ⁶	-73	-236
This work	28	Fund. LO, integer N, mode-switching	2280	10 ^{7.8}	-93 to -96 ⁸	176 to 212 ⁸	3 ⁹	54.65	5.3	0.19 ¹⁰	-61	-245 to -243 ⁸

1) $FOM = 10 \log\left(\frac{\sigma_{t,PLL}^2}{1s} \frac{P_{PLL}}{1mW}\right)$, defined in [40] 2) Estimated from graph. 3) Frequency generation part only. 4) Simulated. 5) Fractional spur. 6) Including pads. 7) Not including generation of the high reference frequency of 2280 MHz. 8) Low-noise mode, used as soon as locking is complete. Fast-locking mode power consumption is 15.2 mW, phase noise at 1 MHz is -84 to -92 dBc/Hz, the RMS jitter is 245 to 433 fs and the FOM is -240 to -235 dB. 9) Fast-locking mode, used only when locking. Low-noise mode lock time is 12 μ s. 10) Including estimated area for implementation if the externally added loop filter is placed on-chip instead.

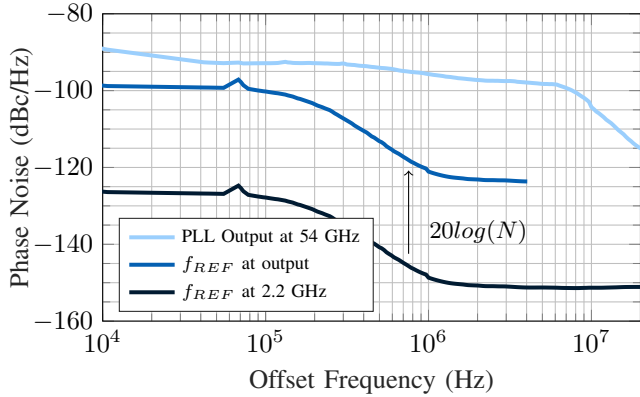


Fig. 19. Measured phase noise of f_{REF} , scaled at output with $20 \log(N)$, and the best-case measured PLL phase noise.

were -95.7 dBc and -103.5 dBc, respectively. The measured in-band phase noise at 1 MHz offset stayed below -93 dBc in all low-noise mode measurements. Since the PLL will be in low-noise mode when used as a clock source, the measured phase noise of this mode will be presented as the overall PLL performance.

The measured noise includes a negligible noise contribution from the frequency reference signal, see Fig. 19. If a CMOS state-of-the-art, low-jitter 2.2 GHz PLL, such as [41], [42], is used as the input reference frequency generator, the integrated jitter is estimated to rise from 176 fs to between approximately 200 and 230 fs.

Separate phase noise measurements were conducted with the current source matching in the CP disabled. They indicate that the technique does help reduce the phase noise, especially

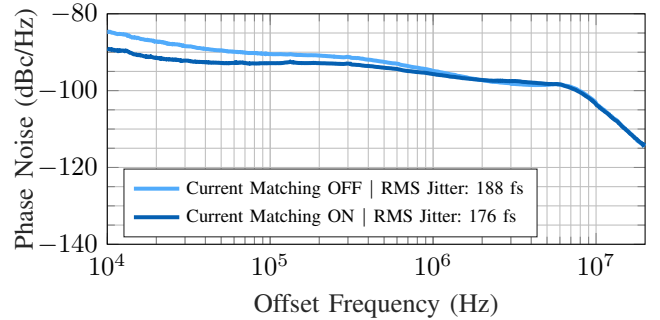


Fig. 20. Measured phase noise of the PLL at 55 GHz in low-noise mode, with the CP current matching ON and OFF.

at lower offset frequencies, as expected. A measurement showing the impact on the phase noise in low-noise mode is shown in Fig. 20.

To estimate the settling time, and to verify concept of the mode-switching PLL, the loop control voltage was measured during settling with a digital oscilloscope. To introduce a step in the PLL, a pulsed input signal was applied to the Sel signal that controls the division ratio of the divide-by-6-or-4 divider in the feedback path, see Fig. 4, while the reference frequency was kept constant. That means that the PLL goes from an unlocked state, when the division ratio times the reference frequency does not fall inside the VCO tuning range, to a locked state. When $Sel = 0$, the total division ratio is equal to 24, and if the loop is then in an unlocked state, the targeted frequency is below the VCO tuning range and the control voltage is at its minimum. When $Sel = 1$, on the other hand, the total division ratio is equal to 36, and

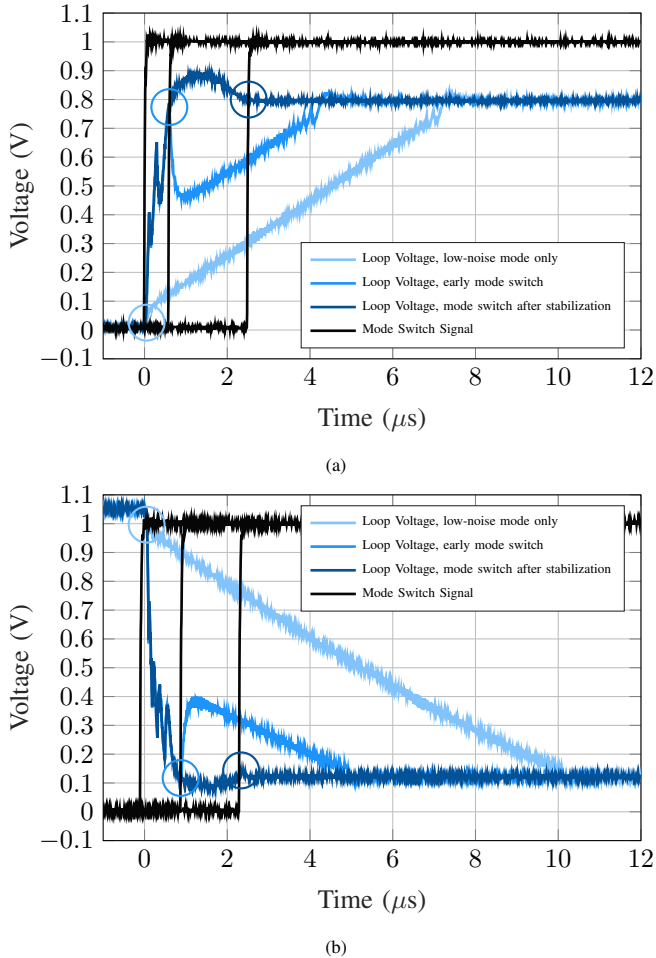


Fig. 21. Measured loop control voltage during settling. Three different cases of timing switching from fast-locking to low-noise mode are shown. (a) Settling to 56.34 GHz. (b) Settling to 53.232 GHz.

if then in the unlocked state the targeted frequency is above the VCO tuning range, and the control voltage is instead at its maximum. Another pulsed signal was used to control the PLL mode switch. In Fig. 21 the settling behaviour with the mode switch activated at different time delays is shown. When both pulsed signals switch at the same time, the settling behaviour will be that of the low-noise mode. When the mode switch signal is delayed, the settling instead starts in fast-locking mode, followed by a switch to low-noise mode. The estimated settling time in low-noise mode is about three times longer than the estimated settling time using fast-locking mode during the first part of the settling. The estimated maximum settling time using fast-locking of $3 \mu\text{s}$ was determined as the PLL settling time. The figure also shows that the switching between modes has minimal impact on the output frequency, and that the best time to switch from fast-locking to low-noise mode is when the frequency is close to stable. However, the measurements also show that since the switch can safely be made at any time, and that any time operating in fast-locking mode improves the settling time significantly, there is no need for complicated algorithms and feedback to control the mode switch mechanism.

The performance of the PLL is summarized in Table II. The PLL figure-of-merit (FOM_{PLL}) is commonly used for wireless communication PLLs, and it is based on the theory in

[40], where the phase noise figure-of-merit (FOM) for VCOs is extended to an entire PLL. Compared to state-of-the-art published mm-wave PLLs, the mode-switching PLL reported in this paper achieves comparable settling time, area and phase noise performance, but at much lower power consumption, which results in a state-of-the-art FOM_{PLL} of -245 dB for this frequency range. Even if the output frequency range is enough to cover the main intended use of the PLL and also enough to demonstrate the architecture, an increased range, attainable with small changes in the VCO, would make it useful for a wider range of applications.

V. CONCLUSION

A novel PLL for mm-wave frequency wireless transceivers is presented, that mitigates the problem of cycle slips during settling by switching between two modes of operation with the same small-signal, but different large-signal properties. Two key building blocks of the PLL include novel circuit techniques. The first is a double injection divide-by-3 circuit which increases the frequency lock range, allowing the power consumption of the mm-wave divider to be robustly scaled down to less than 0.8 mW. The second is the charge pump, which has a replica-based feedback loop to diminish the current mismatch due to channel length modulation, therefore reducing low-frequency PLL phase noise. Measurements show a PLL lock time of about $3 \mu\text{s}$ using the fast-settling mode during the first part of settling, while then operating in low-noise mode achieves a record low power consumption of 10 mW and a state-of-the-art FOM_{PLL} of -245 dB for PLLs in the 60 GHz range.

ACKNOWLEDGMENT

The authors thank STMicroelectronics for the chip fabrication. The authors also gratefully acknowledge Dr. D. Kuylenstierna at Chalmers University of Technology and Rohde & Schwarz for their support with obtaining measurement instruments, and the Chalmers Microwave Electronics Laboratory for providing an environment for the measurements.

REFERENCES

- [1] T. Pollet, M. V. Bladel, and M. Moeneclaey, "BER sensitivity of OFDM systems to carrier frequency offset and Wiener phase noise," *IEEE Transactions on Communications*, vol. 43, no. 2/3/4, pp. 191–193, Feb 1995.
- [2] "IEEE Standard for Information technology–Telecommunications and information exchange between systems Local and metropolitan area networks–Specific requirements - Part 11: Wireless LAN Medium Access Control (MAC) and Physical Layer (PHY) Specifications," *IEEE Std 802.11-2016 (Revision of IEEE Std 802.11-2012)*, pp. 1–3534, Dec 2016.
- [3] W. Wu, R. B. Staszewski, and J. R. Long, "A 56.4-to-63.4 GHz Multi-Rate All-Digital Fractional-N PLL for FMCW Radar Applications in 65 nm CMOS," *IEEE Journal of Solid-State Circuits*, vol. 49, no. 5, pp. 1081–1096, May 2014.
- [4] Y. A. Li, M. H. Hung, S. J. Huang, and J. Lee, "A fully integrated 77GHz FMCW radar system in 65nm CMOS," in *2010 IEEE International Solid-State Circuits Conference - (ISSCC)*, Feb 2010, pp. 216–217.
- [5] "3GPP TR 38.815 V15.0.0 New frequency range for NR (24.25-29.5 GHz)," *3GPP(Release 15)*, pp. 1–22, July 2018.
- [6] A. Axholt and H. Sjöland, "A 60 GHz receiver front-end with PLL based phase controlled LO generation for phased-arrays," *Analog Integrated Circuits and Signal Processing*, vol. 80, no. 1, pp. 23–32, 2014.

- [7] W. El-Halwagy, A. Nag, P. Hisayasu, F. Aryanfar, P. Mousavi, and M. Hossain, "A 28-GHz Quadrature Fractional-N Frequency Synthesizer for 5G Transceivers With Less Than 100-fs Jitter Based on Cascaded PLL Architecture," *IEEE Transactions on Microwave Theory and Techniques*, vol. 65, no. 2, pp. 396–413, Feb 2017.
- [8] S. Ikeda, H. Ito *et al.*, "A -244-dB FOM High-Frequency Piezoelectric Resonator-Based Cascaded Fractional-N PLL With Sub-ppb-Order Channel-Adjusting Technique," *IEEE Journal of Solid-State Circuits*, vol. 52, no. 4, pp. 1123–1133, April 2017.
- [9] G. Rubio-Cidre, A. Badolato, L. Úbeda Medina, J. Grajal, B. Mencia-Oliva, and B. Dorta-Naranjo, "DDS-Based Signal-Generation Architecture Comparison for an Imaging Radar at 300 GHz," *IEEE Transactions on Instrumentation and Measurement*, vol. 64, no. 11, pp. 3085–3098, Nov 2015.
- [10] K. B. Cooper, R. J. Dengler *et al.*, "Penetrating 3-D Imaging at 4- and 25-m Range Using a Submillimeter-Wave Radar," *IEEE Transactions on Microwave Theory and Techniques*, vol. 56, no. 12, pp. 2771–2778, Dec 2008.
- [11] D. A. Robertson, P. N. Marsh *et al.*, "340-GHz 3D radar imaging test bed with 10-Hz frame rate," vol. 8362, 2012, pp. 8362 – 8362 – 11. [Online]. Available: <https://doi.org/10.1117/12.918581>
- [12] R. He, J. Li, W. Rhee, and Z. Wang, "Transient analysis of nonlinear settling behavior in charge-pump phase-locked loop design," in *2009 IEEE International Symposium on Circuits and Systems*, May 2009, pp. 469–472.
- [13] S. Ek, T. Pahlsson *et al.*, "A 28-nm FD-SOI 115-fs Jitter PLL-Based LO System for 24–30-GHz Sliding-IF 5G Transceivers," *IEEE Journal of Solid-State Circuits*, vol. 53, no. 7, pp. 1988–2000, July 2018.
- [14] E. Hegazi, H. Sjöland, and A. A. Abidi, "A filtering technique to lower LC oscillator phase noise," *IEEE Journal of Solid-State Circuits*, vol. 36, no. 12, pp. 1921–1930, Dec 2001.
- [15] T. Forsberg, J. Wernehag, A. Nejdell, H. Sjöland, and M. Törmänen, "Two mm-Wave VCOs in 28-nm UTBB FD-SOI CMOS," *IEEE Microwave and Wireless Components Letters*, vol. 27, no. 5, pp. 509–511, May 2017.
- [16] J. Yuan and C. Svensson, "High-speed CMOS circuit technique," *IEEE Journal of Solid-State Circuits*, vol. 24, no. 1, pp. 62–70, Feb 1989.
- [17] U. Decanis, A. Ghilioni, E. Monaco, A. Mazzanti, and F. Svelto, "A Low-Noise Quadrature VCO Based on Magnetically Coupled Resonators and a Wideband Frequency Divider at Millimeter Waves," *IEEE Journal of Solid-State Circuits*, vol. 46, no. 12, pp. 2943–2955, Dec 2011.
- [18] A. I. Hussein and J. Paramesh, "Design and Self-Calibration Techniques for Inductor-Less Millimeter-Wave Frequency Dividers," *IEEE Journal of Solid-State Circuits*, vol. 52, no. 6, pp. 1521–1541, June 2017.
- [19] H. Wu and L. Zhang, "A 16-to-18GHz 0.18- μ m Epi-CMOS Divide-by-3 Injection-Locked Frequency Divider," in *2006 IEEE International Solid State Circuits Conference - Digest of Technical Papers*, Feb 2006, pp. 2482–2491.
- [20] T. N. Luo, S. Y. Bai, and Y. J. E. Chen, "A 60-GHz 0.13- μ m CMOS Divide-by-Three Frequency Divider," *IEEE Transactions on Microwave Theory and Techniques*, vol. 56, no. 11, pp. 2409–2415, Nov 2008.
- [21] Y. T. Chen, M. W. Li, H. C. Kuo, T. H. Huang, and H. R. Chuang, "Low-Voltage K -Band Divide-by-3 Injection-Locked Frequency Divider With Floating-Source Differential Injector," *IEEE Transactions on Microwave Theory and Techniques*, vol. 60, no. 1, pp. 60–67, Jan 2012.
- [22] H. R. Rategh and T. H. Lee, "Superharmonic injection-locked frequency dividers," *IEEE Journal of Solid-State Circuits*, vol. 34, no. 6, pp. 813–821, Jun 1999.
- [23] B. Razavi, "A study of injection locking and pulling in oscillators," *IEEE Journal of Solid-State Circuits*, vol. 39, no. 9, pp. 1415–1424, Sept 2004.
- [24] H.-H. Hsieh, F.-L. Hsueh *et al.*, "A V-band divide-by-three differential direct injection-locked frequency divider in 65-nm CMOS," in *IEEE Custom Integrated Circuits Conference 2010*, Sept 2010, pp. 1–4.
- [25] M. Abdulaziz, W. Ahmad, M. Törmänen, and H. Sjöland, "A Linearization Technique for Differential OTAs," *IEEE Transactions on Circuits and Systems II: Express Briefs*, vol. 64, no. 9, pp. 1002–1006, Sept 2017.
- [26] R. Y. Chen, "High-speed CMOS frequency divider," *Electronics Letters*, vol. 33, no. 22, pp. 1864–1865, Oct 1997.
- [27] D. J. Allstot, "A precision variable-supply CMOS comparator," *IEEE Journal of Solid-State Circuits*, vol. 17, no. 6, pp. 1080–1087, Dec 1982.
- [28] B. D. Muer and M. S. J. Steyaert, "On the analysis of $\Delta\Sigma$ fractional-N frequency synthesizers for high-spectral purity," *IEEE Transactions on Circuits and Systems II: Analog and Digital Signal Processing*, vol. 50, no. 11, pp. 784–793, Nov 2003.
- [29] —, "A CMOS monolithic $\Delta\Sigma$ -controlled fractional-N frequency synthesizer for DCS-1800," *IEEE Journal of Solid-State Circuits*, vol. 37, no. 7, pp. 835–844, Jul 2002.
- [30] M. G. Johnson and E. L. Hudson, "A variable delay line PLL for CPU-coprocessor synchronization," *IEEE Journal of Solid-State Circuits*, vol. 23, no. 5, pp. 1218–1223, Oct 1988.
- [31] F. Herzel, S. A. Osmany, and J. C. Scheytt, "Analytical Phase-Noise Modeling and Charge Pump Optimization for Fractional-N PLLs," *IEEE Transactions on Circuits and Systems I: Regular Papers*, vol. 57, no. 8, pp. 1914–1924, Aug 2010.
- [32] S. Levantino, G. Marzin, C. Samori, and A. L. Lacaita, "A wideband fractional-n pll with suppressed charge-pump noise and automatic loop filter calibration," *IEEE Journal of Solid-State Circuits*, vol. 48, no. 10, pp. 2419–2429, Oct 2013.
- [33] J.-S. Lee, M.-S. Keel, S.-I. Lim, and S. Kim, "Charge pump with perfect current matching characteristics in phase-locked loops," *Electronics Letters*, vol. 36, no. 23, pp. 1907–1908, Nov 2000.
- [34] X. Yi, C. C. Boon, H. Liu, J. F. Lin, and W. M. Lim, "A 57.9-to-68.3 GHz 24.6 mW Frequency Synthesizer With In-Phase Injection-Coupled QVCO in 65 nm CMOS Technology," *IEEE Journal of Solid-State Circuits*, vol. 49, no. 2, pp. 347–359, Feb 2014.
- [35] V. Szortyka, Q. Shi, K. Raczkowski, B. Parvais, M. Kuijk, and P. Wambacq, "A 42 mW 200 fs-Jitter 60 GHz Sub-Sampling PLL in 40 nm CMOS," *IEEE Journal of Solid-State Circuits*, vol. 50, no. 9, pp. 2025–2036, Sept 2015.
- [36] W. Wu, R. B. Staszewski, and J. R. Long, "A 56.4-to-63.4 GHz Multi-Rate All-Digital Fractional-N PLL for FMCW Radar Applications in 65 nm CMOS," *IEEE Journal of Solid-State Circuits*, vol. 49, no. 5, pp. 1081–1096, May 2014.
- [37] C. H. Tsai, G. Mangraviti, Q. Shi, K. Khalaf, A. Bourdoux, and P. Wambacq, "A 54-64.8 GHz subharmonically injection-locked frequency synthesizer with transmitter EVM between -26.5 dB and -28.8 dB in 28 nm CMOS," in *ESSCIRC 2017 - 43rd IEEE European Solid State Circuits Conference*, Sept 2017, pp. 243–246.
- [38] A. I. Hussein, S. Vasadi, and J. Paramesh, "A 50-66-GHz Phase-Domain Digital Frequency Synthesizer With Low Phase Noise and Low Fractional Spurs," *IEEE Journal of Solid-State Circuits*, vol. 52, no. 12, pp. 3329–3347, Dec 2017.
- [39] T. Siriburanon, S. Kondo *et al.*, "A Low-Power Low-Noise mm-Wave Subsampling PLL Using Dual-Step-Mixing ILFD and Tail-Coupling Quadrature Injection-Locked Oscillator for IEEE 802.11ad," *IEEE Journal of Solid-State Circuits*, vol. 51, no. 5, pp. 1246–1260, May 2016.
- [40] X. Gao, E. A. M. Klumperink, P. F. J. Geraedts, and B. Nauta, "Jitter Analysis and a Benchmarking Figure-of-Merit for Phase-Locked Loops," *IEEE Transactions on Circuits and Systems II: Express Briefs*, vol. 56, no. 2, pp. 117–121, Feb 2009.
- [41] J. Sharma and H. Krishnaswamy, "A dividerless reference-sampling RF PLL with -253.5dB jitter FOM and <-67dBc Reference Spurs," in *2018 IEEE International Solid - State Circuits Conference - (ISSCC)*, Feb 2018, pp. 258–260.
- [42] X. Gao, E. A. M. Klumperink, M. Bohsali, and B. Nauta, "A Low Noise Sub-Sampling PLL in Which Divider Noise is Eliminated and PD/CP Noise is Not Multiplied by N^2 ," *IEEE Journal of Solid-State Circuits*, vol. 44, no. 12, pp. 3253–3263, Dec 2009.



Mohammed Abdulaziz (S'12-M'16) received the M.Sc. degree in 2011 and PhD degree from the Analog RF Group at the Department of Electrical and Information Technology, Lund University, Sweden, in 2016. His master thesis was on digital phase-locked loops and his Ph.D. research was on digitally assisted RF front-ends and analog baseband circuits with a focus on the linearity enhancement of receiver circuits. In 2015, he was a visiting researcher with the Integrated Circuit Design Group, University of Twente, The Netherlands.

He joined as a post-doctoral fellow in Lund University from May 2016 till March 2017 where he worked on mm-wave phase-locked loop frequency synthesizers for 5G communication systems. In March 2017 Mohammed Abdulaziz became a post-doctoral fellow in Chalmers University of Technology and his research included high performance mm-wave 5G front-ends including receivers, transmitters as well as frequency generation circuits. Since August 2018 Mohammed has joined as a researcher in Ericsson Research, Lund, Sweden.



Henrik Sjöland (M'98-SM'10) received the M.Sc. degree in electrical engineering from Lund University, Sweden, in 1994, and the PhD degree from the same university in 1997. In 1999 he was a postdoc at UCLA on a Fulbright scholarship. He has been an associate professor at Lund University since year 2000, and a full professor since 2008. Since 2002 he is also part time employed at Ericsson Research, where he is currently a Senior Specialist. He has authored or co-authored more than 170 international peer reviewed journal and conference papers and

holds patents on more than 25 different inventions.

Henrik Sjöland is currently an associate editor of IEEE Transactions on Circuits and Systems – I, and he has been an associate editor of IEEE Transactions on Circuits and Systems – II and a member of the Technical Program Committee of the European Solid-State Circuits Conference (ESSCIRC). He is a Senior Member of IEEE. He has successfully been the main supervisor of 13 PhD students to receive their degrees. His research interests include design of radio frequency, microwave, and mm wave integrated circuits, primarily in CMOS technology.



Therese Forsberg (S'13-M'18) received the M.Sc. degree in electronics design engineering from Linköping University, Sweden, in 2007. Her master thesis investigated RF coexistence issues when integrating GPS receivers in cell phones. After 6 years of working with the design and validation of analog transceiver RF ASICs for cell phones at Ericsson AB in Lund, Sweden, she joined the Analog RF Group at the Department of Electrical and Information Technology, Lund University, Sweden, as a PhD student. She received the PhD degree in December

2018 with research focus on efficient mm-wave transmitter design in CMOS technology. In January 2019 she joined the RF-ASIC group at Ericsson AB, Lund, Sweden.



Markus Törmänen (S'06-M'10-SM'12) received the PhD degree in Circuit Design in 2010 from Lund University, Sweden. He was a RF Research Engineer at Lund University in 2003-2006; Department of Electrosience (2003-2004) and MAX-lab (2004-2006). He was an assistant professor at Lund University 2010-2013, and since 2014 he has been associate professor and Docent at Lund University. He has authored or co-authored more than 60 international peer reviewed journal and conference papers.

He is Program Director for Electrical Engineering (M.Sc.Eng) at Lund University and he has been awarded the IEEE Senior Member grade. He is also part of the RF group designing the low-level RF system for the European Spallation Source (ESS). His research interests include design of analog, RF, and mm-wave CMOS circuits.